Journal of Materials Research and Technology 32 (2024) 541–549

Contents lists available at ScienceDirect

Journal of Materials Research and Technology

journal homepage: www.elsevier.com/locate/jmrt

Effect of acid mine drainage on the mechanical properties of AISI 1020 carbon steel and AW6060 aluminium

Aguasanta Miguel Sarmiento [a,b,*], Angel Mariano Rodriguez-Perez [c], Jose Miguel Davila [a,b], Maria Luisa de la Torre [a,d]

[a] Department of Mining, Mechanical, Energy and Construction Engineering, University of Huelva, Huelva, Spain
[b] Science and Technology Centre of Huelva (CCTH), University of Huelva, Spain
[c] Department of Engineering, University of Almería, Almería, Spain
[d] Natural Resources, Health and Environment Research Centre (RENSMA), University of Huelva, Spain

ARTICLE INFO

Keywords:
Acid mine drainage
Mechanical properties
Carbon steel
Aluminum
Corrosion
Erosion
Fatigue resistance
Tensile strength
Durability

ABSTRACT

Acid mine drainage severely affects metallic materials due to the high acidity and oxidising capacity of these lixiviates. A study was carried out to evaluate the time evolution of the mechanical properties of AISI 1020 carbon steel and AW6060 aluminium in contact with acid mine drainage. Weight loss, fatigue and tensile strength were evaluated in two different scenarios, one involving erosion corrosion (dynamic scenario) and the other involving chemical corrosion only (static scenario). Over 80 days of exposure in a static scenario, weight loss is almost 2% for aluminium and 0.5% for steel, fatigue strength is reduced by 28% for steel and ultimate tensile strength is reduced by almost 5% for aluminium and by 2.5% for steel. In a dynamic scenario, the weight loss after 4 days of exposure is 30–35% for both materials, the fatigue strength is reduced by almost 50% for steel, the ultimate tensile strength is reduced by 33% for aluminium and by almost 5% for steel. Acid drainage causes an increase in brittleness and a decrease in stiffness of these materials, much more rapidly in a dynamic environment favoured by the effects of erosion corrosion.

1. Introduction

Among the commonly used metallic materials for structural and mechanical components, aluminium and steel are the most widely used due to their versatility and adaptability, although it is well known that these materials undergo corrosion processes that are strongly accelerated in acidic environments [1], including Acid Mine Drainage (AMD). Steel and aluminium degradation is a serious problem for mining companies that profit from polymetallic sulphides at all stages of mining. Mobile machinery, support structures of mineral processing facilities, crushing, grinding, regrinding, classifying machinery, etc., are also subjected to these environments. Other auxiliary machinery such as pumping and ventilation equipment, augers and drilling/blasting equipment, control panels, etc., can also be affected [1].

In addition, aluminium alloys are used extensively in the construction of aircraft structures. Aluminium sheet is easily fabricated into the machined skins, honeycomb rudder skins, fuselage, payload bay doors, crew cabin, wings and body flap of NASA's Space Shuttle. It is well known that these materials can be damaged by aggressive environments, suffering corrosion processes that are greatly accelerated in acidic environments [1], such as acid mine drainage (AMD). For more than twenty years, specialists from NASA, ESA and others have been coming regularly to Rio Tinto (Huelva, Spain) to study the subsurface and the acid river. In this valley, they also test their equipment and prepare for their missions to Mars, given the similarity of the physicochemical characteristics of these environments, produced by the oxidation of polymetallic sulphides, to that planet [2].

The mining of polymetallic sulphides, and more specifically Fe-sulfides, generates an acidic leachate with a high concentration of sulphates and dissolved metals, which is a worldwide problem [3], not only because of the pollution it generates and its direct impact on the aquatic environment [4–10], but also because of the number of indirect problems it causes. In this type of mining there are a large number of installations and machines made of steel and aluminium.

Acid mine drainage occurs when metal sulphides, initially in anaerobic conditions, are exposed to atmospheric oxygen and water. The main metallic sulfides found in mine wastes and susceptible to oxidation are pyrite and pyrrhotite, but there are many other sulphides

* Corresponding author. Department of Mining, Mechanical, Energy and Construction Engineering, University of Huelva, Huelva, Spain.
E-mail address: amsarmiento@uhu.es (A. Miguel Sarmiento).

https://doi.org/10.1016/j.jmrt.2024.07.099
Received 8 April 2024; Received in revised form 1 July 2024; Accepted 17 July 2024
Available online 24 July 2024

whose oxidation products release elements such as arsenic, copper, cobalt, cadmium, chromium, nickel, lead, etc. In addition, the acidic hydrolysis of the rock through which these acid leaches flow introduces into the solution, in greater or lesser abundance, elements such as Ca, Al, Mg, Mn, K, Na, etc, in such a way that this type of leachate is a very common type of leachate, so that this type of acid leachate can contain concentrations of up to 60000 mg/L of Fe, 2400 mg/L of Al, 860 mg/L of Zn, 800 mg/L of Cu, 742 mg/L of As, 187000 mg/L of sulphates, among others, and pH values that can even reach negative values [6,11], as an elementary indicator of the aggressiveness of the medium.

These leachates can also contain high numbers of microorganisms [12,13], which accelerate the oxidation rate of iron sulphides [14,15]. Thus, acid mine drainages have a highly oxidising character, with redox potentials that can exceed 700 mV [6]. Examples of these microorganisms include Acidithiobacillus ferrooxidans (A. f.), Thioacillus thiaparus, Leptospirillum ferrooxidans, Acidthiobacillus thiooxidans, etc. Both A. ferrooxidans and Leptospirillum ferrooxidans are iron oxidising bacteria (IOB) [16]. Microorganisms are one of the main contributors to metal corrosion (Microbiologically influenced corrosion, MIC), and are involved in electrochemical corrosion processes [17,18].

Corrosion of metals is an electrochemical process in which the metal is converted to an oxide or any other compound with a higher oxidation number. When the metal (which acts as the anode) is in an aqueous medium in the presence of oxygen or another element with a higher standard reduction potential (which acts as the cathode), oxidation of the metal occurs, releasing electrons and reducing the oxygen in the air and/or the oxidising element. The ions formed at the anode undergo further oxidation to form metal oxides. This electrochemical process is accelerated in acidic media because protons act as catalysts for the reaction, and even more so if the medium contains Fe [19].

There are a large number of dissolved elements in acid mine drainage that have the ability to oxidise solid Fe and Al (zero valent). Elements in solution such as Cu^{2+}, Co^{2+}, Ni^{2+}, Sn^{2+}, Pb^{2+}, SO_4^{2-}, Fe^{3+} and $O_{2(g)}$ in acidic media have a standard reduction potential capable of oxidising Fe (s), and Mn^{2+}, Zn^{2+} and Fe^{2+} can additionally oxidise Al(s). The Fe^{2+} resulting from this reaction is rapidly oxidised to Fe^{3+} forming a hydrated Fe oxide (Fe_2O_3-nH_2O) which has the ability to expand, allowing the attack to penetrate into the interior after oxidation [20]. Aluminium has good corrosion resistance due to the passive oxide layer that forms on its surface. However, it is less resistant in acidic waters and/or waters containing heavy metal ions (as in the case of acid mine drainage). Furthermore, in acidic media, the oxide layer formed on the surface of aluminium has no ability to passivate due to its amphoteric behaviour. Thus, when aluminium oxidation occurs at a pH below 3.5, an ionic hydroxide is formed and remains in solution, whereas when it occurs at a pH above 3.5, a solid oxide is precipitated [20].

Chemical processes are not the only effects that occur in the degradation of these materials. When materials are in a scenario with water movement, such as a stream bed or the movement of water generated in a mining facility, it is also necessary to consider the processes of corrosion by erosion of these materials [21] due to the impact of particles on the surface of the metal. Acid mine drainage is characterised by a high concentration of total dissolved solids, which can reach levels of the order of 3.25 g/L [11]. These particles would attack the metal surface through a directional distribution due to the water flow and will depend mainly on the concentration of dissolved material and the velocity of the water flow [22]. There have been many investigations of erosion corrosion on steels [23,24] and aluminium alloys [25,26], the mechanisms of which have been extensively explained [25].

This research evaluates the extent to which acidic environments affect the durability of the defined metallic materials and to evaluate the differences in the degradation rate in real situations such as materials exposed in a static scenario where there is no erosion corrosion, for example, installations inside the gallery of a mine, or in a dynamic scenario where erosion corrosion must be taken into account, for example, constructions in the bed of an acid stream. The results of this research are intended to provide insight into the hazardousness of the use of these materials in acidic mining environments.

2. Methodology and tests

2.1. Field and laboratory tests

A total of 252 cylindrical AISI 1020 carbon steel specimens and 66 cylindrical AW 6060 aluminium specimens with a diameter of 8 mm and a total length of 145 mm, were prepared according to the specifications of the UNE-EN ISO 6892-1 standard. The composition of these materials according to the manufacturer is shown in Table 1. All samples were rinsed with distilled water, degreased in absolute ethanol, air dried in a desiccator and weighed on a precision balance (Radwag, Polska, ±0.0001 g). After weighing, they were prepared with a special adhesive tape for work in aggressive environments to protect the gripping surface of the jaws.

For the experiments carried out in a dynamic scenario, a total of 30 AW6060 aluminium samples and a total of 75 AISI 1020 carbon steel samples were introduced into the Aguas Agrias stream, which is heavily affected by acidic leachates from the Tharsis Mining Complex (Iberian Pyrite Belt, Huelva, Spain). Table 2 shows the history of average values of some of the parameters measured in the stream, which has an average pH of 2.6, a potential of 660 mV and average concentrations of 12 g/L of sulphates, 1.2 g/L of Fe, 191 mg/L of Zn, etc. The average net acidity is 5700 mg/L as $CaCO_3$ according to calculations described by Ref. [24].

The specimens were arranged so that they were suspended in the water perpendicular to the flow, held in place by a 0.3 mm nylon thread with a resistance of 12.4 kg.

The static tests were carried out in the laboratory using plastic containers filled with water from the same stream (Table 2). A total of 144 carbon steel specimens and 24 aluminium specimens were immersed vertically. For this purpose, holes were drilled in the to hold the metal specimens, leaving free holes to allow oxygen to enter.

After removal of the specimens in both scenarios, they were rinsed, dried and weighed prior to the experiments. The length and cross-section of the specimens were measured using a digital caliper. The corrosion rates of carbon steel and aluminium were assessed from the specific weight loss based on the exposed surface area of the specimen for which the section and length measurements were taken using a caliper. The corrosion rate (mm/year) was calculated using equation (1) described by Ref. [18]:

$$V_c = \frac{87600\ \Delta m}{\rho\ A\ t} \tag{1}$$

Where Vc, Δm, ρ, A and t were corrosion rate (mm/year), weight loss (g), density (g/cm^3), area of specimens (cm^2) and exposition time (h), respectively.

2.2. Surface roughness analysis

The surface roughness analysis was carried out with the help of Mitutoyo Surftest SJ-210 surface roughness tester. The calibration of the device was performed on a roughness standard sample $Ra = 2.97$ μm. The analysis was carried out at three different points on 5 specimens from each series. The average reading of each parameter is calculated in order to ensure the accuracy of the measurements and the surface coverage. The following surface roughness parameters were measured and recorded: arithmetic mean roughness value (Ra), mean roughness depth (Rz) and root mean square roughness (Rq). All analyses were carried out at a measurement speed of 0.5 mm/s and cut-off length (λc) of 0.8 mm.

Table 1
Chemical composition of the AISI 1020 carbon steel and AW6060 aluminium.

AISI 1020	C	Mn	P	S	Si		
(%)	0.18–0.23	0.30–0.60	<0.04	<0.05	0.15–0.30		
AW6060	Si	Fe	Cu	Mn	Cr	Zn	Ti
(%)	0.3–0.6	0.1–0.3	<0.1	<0.6	<0.5	<0.15	<0.1

Table 2
History of average values of some parameters measured in the Aguas Agrias Stream [6].

	pH	Eh	EC	SO4	Al	Ca	Mg	Mn	Cu	Fe	Fe^{2+}	Zn	Si	Cd	Co	Ni	Pb	NA
2002	2.48	654	11.6	13302	542	145	1044	107	20	818		145	6.47	431	6068	4840	136	5055
2003	2.60	648	15.2	14355	823	217	1374	137	33	1759	76	267	24.3	669	8046	5297	195	8505
2004	2.72	668	9.23	12124	468	245	1333	106	49	1146	694	215	23.7	648	6853	4626	499	5268
2005	2.57	682	10.3	12423	423	220	926	105	39	1092	262	158	11.5	526	7234	3954	223	4872
2006	2.64	650	9.34	8513	369	207	865	75	44	1168	604	169	27.7	488	4818	2980	163	4651

Eh: redox potential (mV); EC: electrical conductivity (mS/cm); NA: Net acidity as $CaCO_3$.
All values in mg/L except Cd, Co, Ni y Pb in mg/L.

2.3. Fatigue test on carbon steel AISI 1020

In order to obtain results with a confidence level greater than 85% and a margin of error of 15%, it is necessary to test a total of 23.04 specimens by rotating bending. For the experience carried out in the static scenario, a total of 30 specimens collected after 20, 40, 60 and 80 days of immersion in AMD were tested. For the experience conducted in the dynamic scenario, the specimens were removed from the river after 4 and 7 days.

The fatigue tests were carried out using a Gunt Hamburg WP 140 rotary machine, which rotates the metal at a constant speed of 3000 rpm and applies a force at one end ranging from 10 N to 300 N. To generate the S–N curves, the applied force was reduced in steps of 10 N from 300 N to 240 N and every 5 N from 240 N to 150 N. The specimen was clamped in a vice at one end, occupying 40 mm of the piece and leaving a total length of 105 mm free, thus producing a linear distribution of the moment with the maximum value at the clamped end.

2.4. Tensile test on carbon steel AISI 1020 and aluminium AW6060

Five aluminium specimens were tensile tested after being immersed in AMD in a static scenario for a total of 20, 40 and 80 days. Similarly, 5 aluminium specimens were tested after being immersed in the river for a total of 5, 24, 48, 72 and 96 h.

Similarly, 5 carbon steel specimens were tensile tested after being immersed in AMD in a static laboratory environment for 20, 40, 60 and 80 days. A further 5 specimens were tested after 4 and 7 days of river exposure.

Tensile tests were performed statically using universal equipment (Servosis ME 403 of 200 kN). The specimens were clamped at their ends with two grips for cylindrical sections and the tensile force was applied at a constant speed of 0.5 kN/s, according to the requirements of standard UNE-EN ISO 6892–1: 2020. To determine of the modulus of elasticity, limits close to 15% and 55% of the maximum load were used, depending on the course of each test.

2.5. FESEM microscopy and EDS analysis

Field Emission Scanning Electron Microscope (FESEM) was used to observe the corrosion products. X-ray energy dispersive spectrometry (EDS) was used to analyse the chemical composition of the corrosion products formed. For this purpose, small pieces of the resulting specimens were cut, cleaned, and embedded in epoxy resin.

3. Results and discussion

From the results obtained in the tests carried out, the evolution of the fatigue and static tensile strength of the AISI 1020 carbon steel and of the static tensile strength of the AW6060 aluminium exposed to acid mine drainage has been evaluated in two different scenarios, one in which the material is exposed to contact with the AMD without erosion corrosion (static scenario) and another in which the water is in constant movement due to the natural flow of the stream where the material has been exposed (dynamic scenario).

3.1. Weight loss, corrosion rate and surface roughness

The photographs in Fig. 1 show the appearance of carbon steel and aluminium specimens after exposure to AMD in both static and dynamic scenarios. The carbon steel specimens are not shown after exposure in the static scenario because no significant change in material degradation was observed. Both materials show significant visible degradation within a few hours of exposure, particularly in the dynamic scenario. In the case of aluminium, the degradation is initiated by pitting corrosion in localised areas of the surface, whereas in the case of carbon steel, oxidation occurs over the entire exposed surface.

The surface roughness analyses are presented in Table 3. It can be seen that the measured parameters increase with the exposure time for both materials, which is much more evident in the dynamic scenario. After 960 h of exposure in a static scenario, Ra increases more than three times and more than 1.5 times its initial value for aluminium and steel respectively. In a dynamic scenario, the measured parameters are outside the analysis range for aluminium after 24 h of exposure due to the significant degree of degradation, as can be seen in Fig. 1.

The uneven cross-sectional flow of the water in the stream means that the metal does not lose material uniformly along the specimens, which makes it difficult to calculate the cross-section of the specimens. In order to minimise errors, all specimens were weighed individually and up to 8 values of their diameter were taken along the specimens. The area and corrosion rate of each specimen was calculated using the average of these measurements. Fig. 2 shows the evolution of weight loss and corrosion rate with exposure time for both materials studied in a dynamic scenario. It shows the maximum, minimum and average values obtained in each temporal series of exposed specimens. The longer the exposure time, the more heterogeneity was observed in the degradation of the samples and, consequently, in the results, especially for carbon steel.

Aluminium samples show a progressive weight loss with time in a dynamic scenario, being more pronounced after 50 h. This lower weight loss during the first hours of exposure may be related to the precipitation

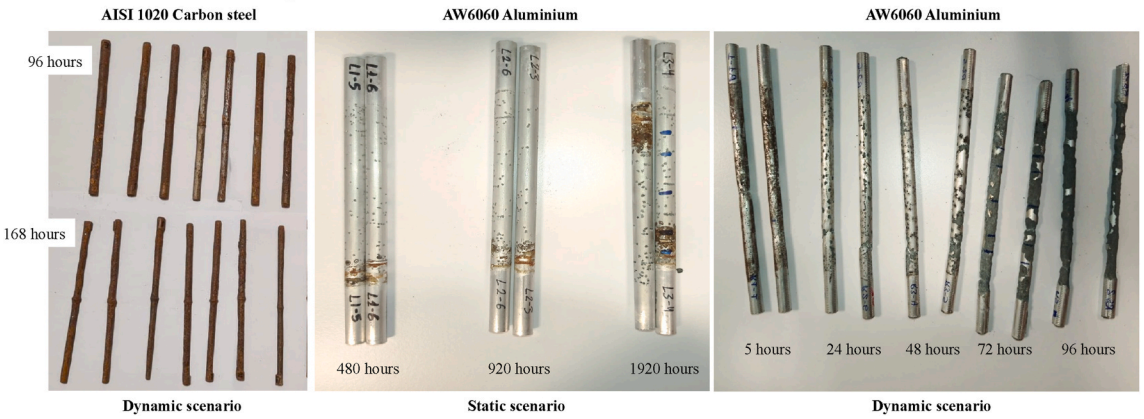

Fig. 1. Appearance of AISI 1020 carbon steel and AW6060 aluminium specimens after AMD exposure.

Table 3
Average values of surface roughness analysed on AW6060 aluminium and AISI 1020 carbon steel specimens before and after exposure to acid mine drainage in the two scenarios studied (n = number of specimens tested).

Static scenario							
Aluminium AW6060				Carbon steel AIS 1020			
Exposure time (h)	Ra (μm)	Rq (μm)	Rz (μm)	Exposure time (h)	Ra (μm)	Rq (μm)	Rz (μm)
0 (n = 15)	0.231	0.313	1.878	0 (n = 15)	0.620	0.798	4.855
480 (n = 15)	0.498	0.641	3.722	480 (n = 15)	0.809	1.174	5.760
960 (n = 15)	0.773	1.009	5.711	960 (n = 15)	0.975	1.291	7.000
1920 (n = 15)	1.164	1.584	9.111	1440 (n = 15)	1.917	2.441	11.51
				1920 (n = 15)	2.013	2.527	12.40
Dynamic scenario							
Aluminium AW6060				**Carbon steel AIS 1020**			
Exposure time (h)	Ra (μm)	Rq (μm)	Rz (μm)	Exposure time (h)	Ra (μm)	Rq (μm)	Rz (μm)
5 (n = 15)	0.642	0.828	3.995	96 (n = 15)	6.257	7.835	32.32
24 (n = 15)	>360	>360	>360	168 (n = 15)	10.31	12.40	47.62
>24	>360	>360	>360				

of copper on the specimen surface by an electrolytic process, a process that also occurs on the surface of carbon steel specimens [5], cushioning the degradation of the material at the beginning of the exposure. For the dynamic scenario chosen, and despite the fact that the samples were not taken at the same time interval, the weight loss of the two materials studied does not seem to show a significant difference after 100 h of exposure (blue circle for steel and red square for aluminium in Fig. 2), evolving in a similar way over time, losing around 30–35% of material at 100 h of exposure for both materials. The corrosion rate recorded after 100 h of exposure of the two materials suggests that the time evolution of the degradation of the two materials is also similar, around 60 mm/year. For the carbon steel, a decrease in the corrosion rate is observed after 7 days of exposure, as the weight loss continues to increase, but not at the same rate. These results suggest that the degradation of the metallic materials studied, exposed in a dynamic scenario with a water flow with AMD characteristics, is mainly due to the effects of erosion on the corrosion products of the metallic materials.

Fig. 3 shows the time evolution of the maximun, minimum and average weight loss and degradation rate of the samples after removal from the container in which they had been immersed in a static scenario. In this case, a greater weight loss is observed in the aluminium samples than in the steel samples, so that before one month the aluminium has lost 1.2% of its weight, while the steel has lost 0.1% of its initial weight. After approximately 3 months of exposure in a static scenario, aluminium and carbon steel have lost 1.8% and 0.5% of their initial weight respectively.

It is observed that, in a static scenario, the weight loss of aluminium is more pronounced in the first few days and decreases with the exposure time, so that the degradation rate decreases from 0.36 mm/year at the beginning of the experiment to 0.15 mm/year after three months. This is due to the electrolytic reaction that takes place, oxidising the zero-valent Al to Al^{3+} and producing hydrogen gas at the cathodic sites. This causes the pH to increase so that the aluminium dissolves in the acid, forming the ionic complex $[Al(H_2O)_6]^{3+}$ at pH below 3.5 and the solid complex $Al(OH)_3(H_2O)_3$ above pH 3.5 [20]. The latter oxide slows down the

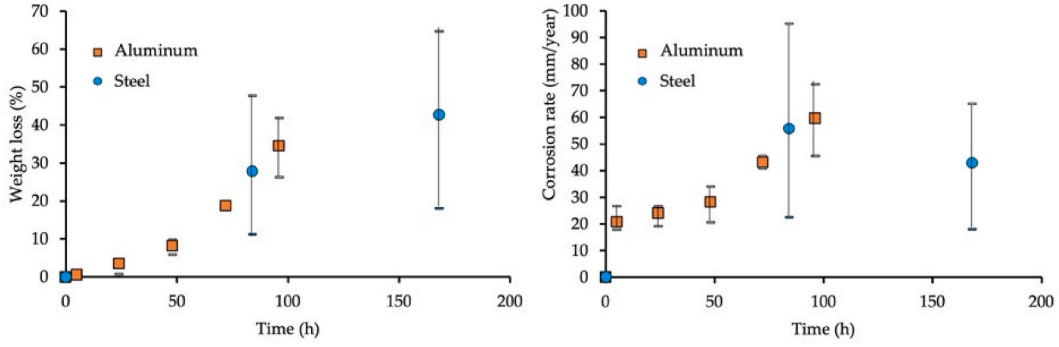

Fig. 2. Time evolution of weight loss (%) and corrosion rate (mm/year) of AISI 1020 carbon steel and AW6060 aluminium specimens exposed to AMD in a dynamic scenario (stream bed). The graphs show the range of values obtained and the average value for each time series of specimens analysed.

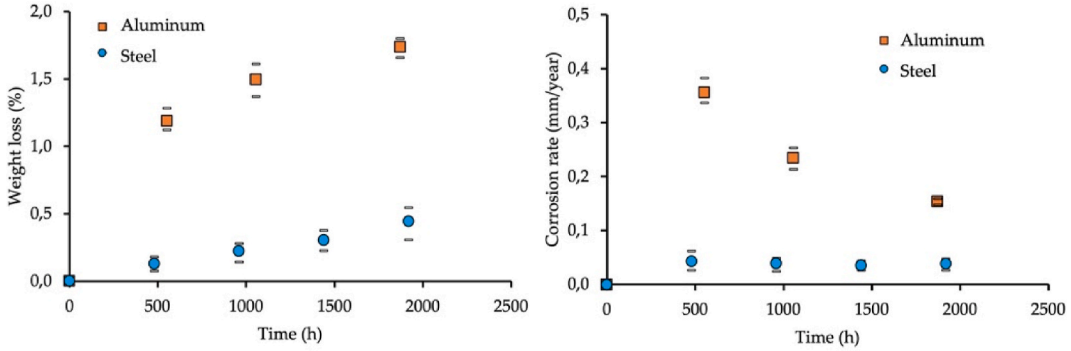

Fig. 3. Time evolution of weight loss (%) and corrosion rate (mm/year) of AISI 1020 carbon steel and AW6060 aluminium specimens exposed to AMD in a static scenario (laboratory). The graphs show the range of values obtained and the average value for each time series of specimens analysed.

oxidation of aluminium. The generation of hydrogen gas also occurs at the cathodic sites of carbon steel and therefore also increases the pH, leading to the precipitation of iron hydroxides on the surface of the solid metal. The corrosion rate of carbon steel is not as high as that of aluminium, but it does not decrease because the oxide layer that forms is very porous, allowing oxidation to continue.

3.2. Fatigue and tensile strength of AISI 1020 carbon steel specimens

From the results of the fatigue tests carried out on AISI 1020 carbon steel specimens exposed to AMD in a static scenario, the S–N curves in Fig. 4A are obtained for 0, 20, 40, 60 and 80 days of exposure. All the specimens were tested to failure, and none were obtained at infinite life. The curve shows the variation in fatigue strength for different exposure times to acid mine drainage.

The S–N curves show the relationship between applied stress and life to failure. The results obtained for a static scenario do not show very significant differences in fatigue strength over the time studied, but an enlargement of the region highlighted in Fig. 4A shows a reduction in fatigue strength, particularly at the beginning of the test (Fig. 4B). The results indicate a reduction in fatigue strength of carbon steel of 14% (at 20 days exposure), 20% (at 40 days), 24% (at 60 days) and 28% (at 80 days) of carbon steel exposed to AMD in a static scenario.

The reduction in the service life of carbon steel is due to defects caused by oxidation at anodic points on the surface of the metal, where a stress concentrator is created and the appearance of micro-cracks that progress to the detachment of the degraded material.

The same applies to the fatigue tests carried out on the samples exposed to AMD in a dynamic scenario, where a significant reduction in fatigue strength is observed (Fig. 5). For a typical number of cycles of 100,000, the fatigue strength is reduced by 48% after 4 days and by 63% after 7 days, significantly reducing the percentage life of the specimens.

The results obtained indicate that the fatigue life of AISI 1020 carbon steel is reduced by almost 30% in less than 3 months in a static scenario and by 63% in just one week of exposure in a dynamic scenario.

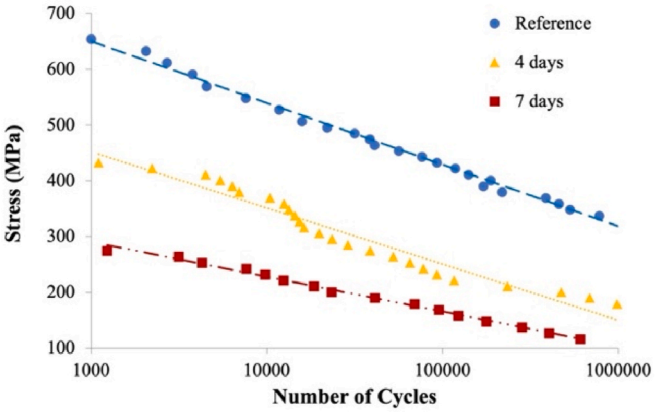

Fig. 5. S–N curves of fatigue tests of AISI 1020 carbon steel specimens exposed for 0 (Reference), 4 and 7 days to AMD in a dynamic scenario (stream bed).

Static tensile tests performed on AISI 1020 carbon steel specimens exposed to AMD in the two scenarios studied reveal interesting characteristics. Fig. 6 shows the time evolution of the values obtained for the ultimate tensile strength, yield tensile strength and Young's modulus of the specimens tested after exposure to AMD in both static and dynamic scenarios. The minimum ultimate strength of AISI 1020 carbon steel, as stated by the manufacturer, is 395 MPa and indicates the maximum stress that the material can withstand under tension before breaking.

The mean ultimate strength obtained decreases with exposure time in both scenarios up to 2.5% at 80 days in the static scenario and up to 4.6% at 7 days in the dynamic scenario. Compared to the significant

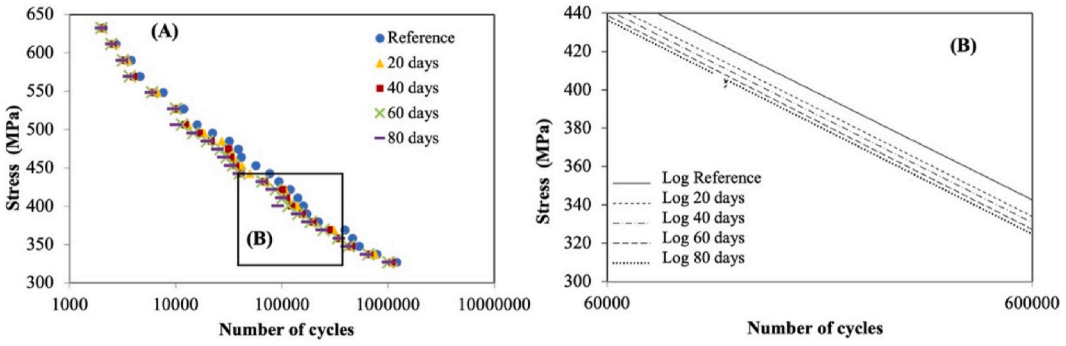

Fig. 4. (A) S–N curves of fatigue tests of AISI 1020 carbon steel specimens exposed for 0 (Reference), 20, 40, 60 and 80 days to AMD in a static scenario (laboratory). (B) Increase of the highlighted area in Figure A.

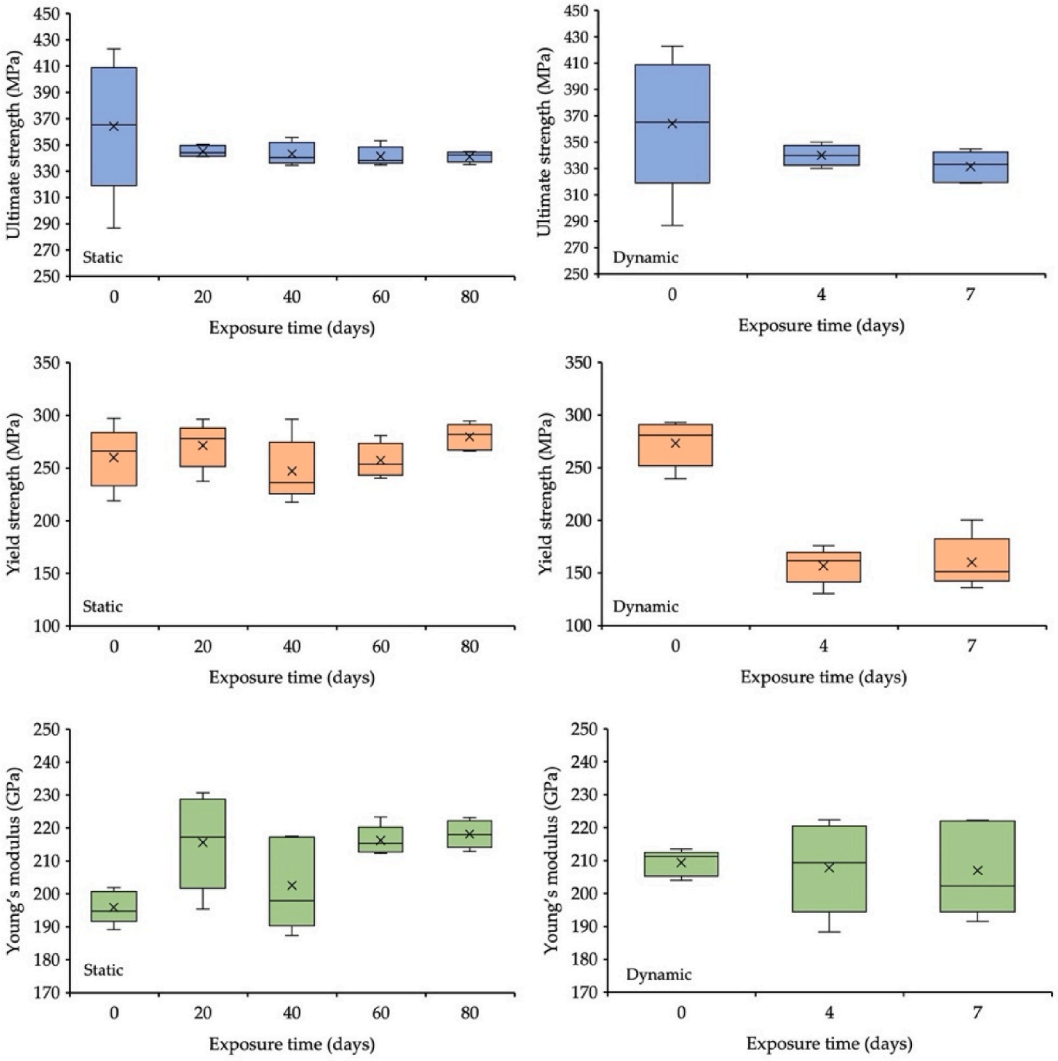

Fig. 6. Box and whisker plots showing the time evolution of the values obtained for the ultimate tensile strength, yield tensile strength and Young's modulus of the tested AISI 1020 steel specimens exposed to AMD in the static scenario (laboratory) and dynamic scenario (stream bed). The number of specimens tested was 5 for each exposure time.

reduction in durability and weight loss, the reduction in ultimate strength after 7 days of exposure in AMD in a dynamic scenario does not seem to be too drastic and therefore does not affect the brittleness of the material too much.

The yield tensile strength of AISI 1020 carbon steel has a minimum value of 294.7 MPa according to the manufacturer. The value of this material is practically unchanged during AMD exposure in a static scenario (Fig. 6), while it decreases by 16% and 21% after 4 and 7 days, respectively, in a dynamic scenario. Regarding the Young's modulus (190–200 GPa depending on the manufacturer), the average values increase by up to 10% of their reference value in the static scenario, while they remain almost unchanged in the dynamic system (Fig. 6). The values obtained for ultimate strength and modulus of elasticity differ relatively little from the reference value, although the fact that the modulus of elasticity tends to increase slightly as the ultimate strength decreases would imply that the material is slightly more brittle and stiffer.

3.3. Tensile strength of AW6060 aluminium specimens

Tensile tests carried out on aluminium specimens exposed to acid drainage show very different data to those found for carbon steel specimens. Fig. 7 shows the time evolution of the values obtained for the ultimate tensile strength, yield tensile strength and Young's modulus of Al AW6060 exposed to AMD in a static and dynamic scenario. The ultimate strength decreases significantly in the dynamic scenario (Fig. 7), so that after 24 h the ultimate strength of the aluminium decreases by 10% of the initial value and by 33% in only 96 h of exposure. In the static scenario, the ultimate strength decreases by 4.7% after 80 days of exposure. These results indicate that the material becomes more brittle with exposure to acid drainage.

A similar situation occurs for the yield strength, with a decrease of 11% in the static scenario at 80 days of exposure and 36% at 96 h in the dynamic scenario (Fig. 7). A decrease in Young's modulus is also observed in both scenarios, with a decrease of 11% in the static scenario after 80 days of exposure and 26% in the dynamic scenario after 96 h of exposure.

From the results obtained, it can be deduced that the investigated mechanical properties of AW6060 aluminium are severely degraded when the material is in contact with acid mine drainage, reducing the stiffness of the material and increasing its brittleness.

3.4. Comparison of the reduction in mechanical properties of AISI 1020 carbon steel and AW6060 aluminium

Table 4 shows the mass loss and the variation of the values obtained

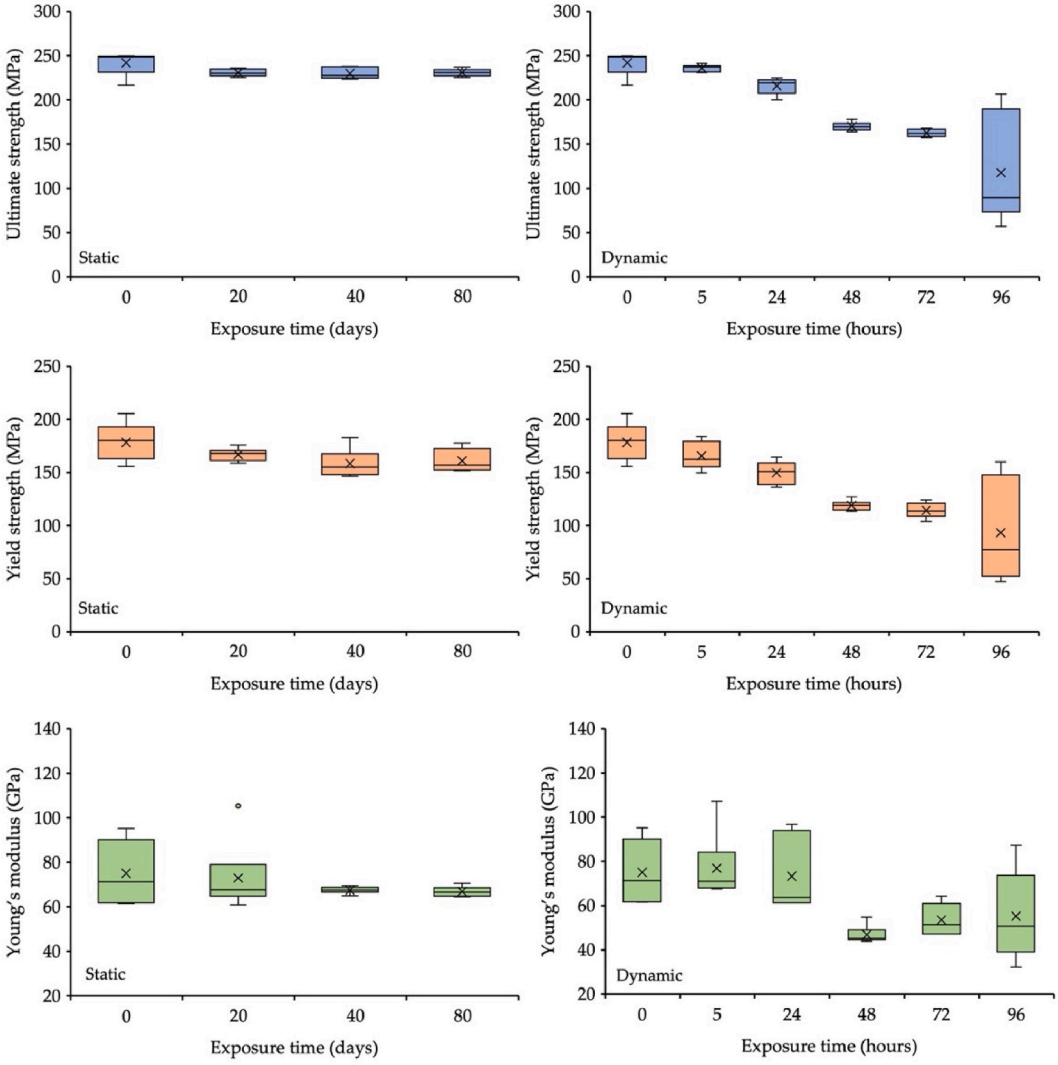

Fig. 7. Box and whisker plots showing the time evolution of the values obtained for the ultimate tensile strength, yield tensile strength and Young's modulus of AW6060 aluminium specimens exposed to AMD in the static scenario (laboratory) and dynamic scenario (stream bed).
The number of specimens tested was 5 for each exposure time.

in the tests carried out for both materials studied after being exposed to AMD for 80 days in a static scenario and for 4 days in a dynamic scenario.

The results show that, for the same exposure time, in a dynamic scenario the weight loss is similar for both materials, whereas in a static scenario the weight loss evolves differently. These results indicate that in a dynamic scenario the degradation produced in both materials has a greater effect due to the influence of erosion corrosion.

The degradation suffered by aluminium in both scenarios is much higher than that suffered by carbon steel, as would be expected due to its greater reactivity to corrosion in an acidic environment, which significantly reduces the mechanical properties evaluated, making it less rigid and more fragile. Scanning electron microscopy observations on the corrosion products of an AW6060 aluminium specimen exposed to AMD suggest that AMD degradation of the aluminium produces defects that indicate an attack mainly on the grain boundaries of the material (Fig. 8), producing voids with metallic Cu incrustations.

Carbon steel degradation reacts in the same way than aluminium degradation, but with a much smaller reduction in its mechanical properties, so that its brittleness decreases slightly while its stiffness remains practically unchanged. It could therefore be said that AMD degradation of AISI 1020 carbon steel does not significantly affect the mechanical properties of the material during the exposure time studied, in terms of elasticity, brittleness and life for degradation in a static scenario, while it does affect life in a dynamic scenario, possibly because this degradation only occurs in the most superficial layers of the material (Fig. 9A). Scanning Electron Microscope (FESEM) observations of a cross section of a steel specimen affected by AMD show the presence of microcracks from the affected surface towards the interior of the specimen (Fig. 9B), possibly causing encapsulation of the material and leading to material loss (Fig. 9C).

Table 4
Summary of test results for mechanical materials affected by AMD for the same exposure time in both scenarios.

	AW6060 Aluminium		AISI 1020 carbon steel	
	Static (80 d)	Dynamic (4 d)	Static (80 d)	Dynamic (4 d)
Weight loss	1,8%	30%	↓0,5%	35%
Fatigue strength	–	–	↓28%	↓48%
Ultimate strength	↓4,7%	↓33%	↓2,5%	↓4,6%
Yield tensile strength	↓11%	↓36%	0,4%	↓16%
Young's modulus	↓11%	↓26%	↑10%	0,7%

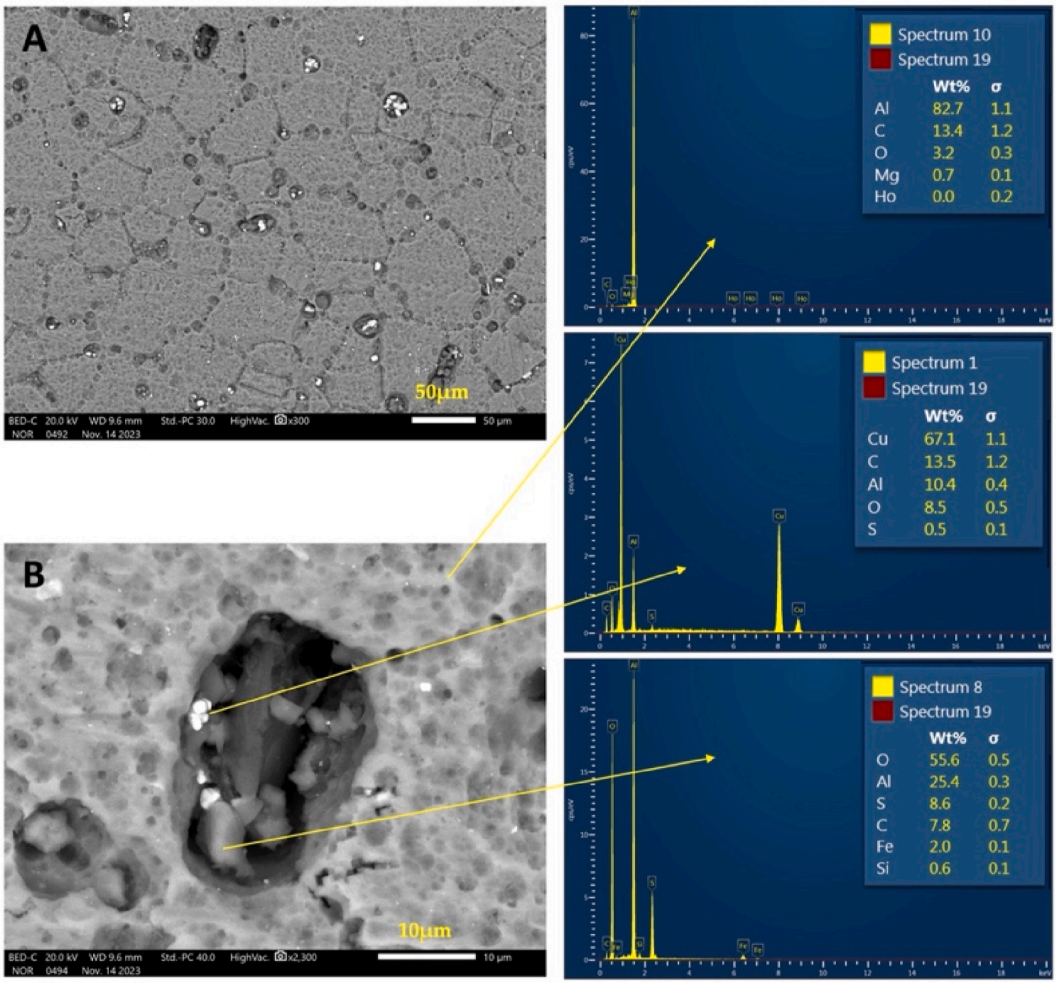

Fig. 8. A) FESEM of the surface of an aluminum specimen affected by AMD. (B) Detail of a hole where Cu and aluminum sulphate precipitates are housed.

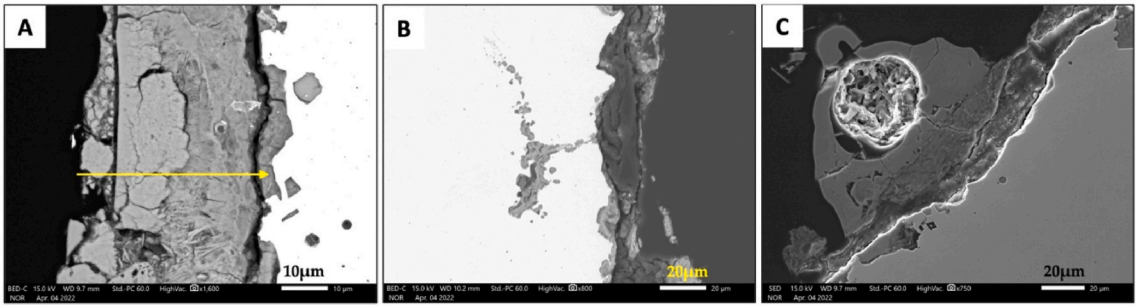

Fig. 9. Scanning electron microscopy (FESEM) of the cross section of a carbon steel specimen affected by AMD.

Failure of the fatigue-tested material occurs in several stages, with failure starting when a flaw appears and progressing to failure. This process can also begin at locations that have some type of irregularity such as inclusions, surface discontinuities, etc., but this last factor can be ignored as all the specimens tested are from the same material. The defect created by the oxidation of the metal at the anodic sites is a stress concentrator and the site of microcrack initiation, explaining the significant reduction in fatigue strength.

4. Conclusion

In a static scenario where the AMD is not moving, Al AW6060 experiences a rapid weight loss in the first few days of exposure, which decreases as the acidity of the water is consumed due to the change in solubility of the aluminium corrosion product. Carbon steel loses less weight than aluminium, but the corrosion rate remains constant due to the porosity of the iron corrosion products. When acid drainage is flowing, AW6060 aluminium and AISI 1020 carbon steel experience similar weight loss with exposure time, so the effects of erosion corrosion are the same on both materials. AW6060 aluminium exposed to AMD becomes more brittle and less stiff with exposure time, much more so in a dynamic scenario where water flow is present. The reason for this is that the degradation of the aluminium creates defects that indicate an attack mainly at the grain boundaries of the material, increasing the porosity of the metal. Acid leachates slightly reduce the brittleness of AISI 1020 carbon steel, but do not affect the stiffness of the material

because the oxidation proceeds in layers, affecting the superficial parts of the metal. On the other hand, it significantly reduces the service life due to the defects caused by oxidation at the anodic sites on the surface of the metal, where a stress concentrator is created and the onset of microcracks that progress to detachment of the degraded material.

The results show the serious problems that would result from the use of these materials for the use of mechanical components in a sulphide mining environment, not only because of the significant reduction in the lifetime of such components, but also because of the implications for human safety.

Declaration of competing interest

The authors declare that they have no known competing financial interests or personal relationships that could have appeared to influence the work reported in this paper.

Acknowledgments

This work has been supported by MCIN/AEI/10.13039/501100011033/FEDER, UE, throughout the project PID2021-123130OB-I00. Authors thank the reviewers for their valuable comments.

References

[1] Javaherdashti R, Nikraz H. On the role of deterioration of structures in their performance; with a focus on mining industry equipment and structures. Mater Corros 2010;61:885–90. https://doi.org/10.1002/maco.200905515.
[2] Cannon HN, Stoker CR, Dunagan SE, Kavis K, Gómez-Elvira J, Glass BJ, Lemke LG, Miller D, Bonaccorsi R, Branson M, Christa S, Rodriguez-Manfredi JA, Mumm E, Paulsen G, Roman M, Winterholler A, Zavaleta JR. Marte: technology development and lessons learned from a Mars drilling mission simulation. J Field Robot 2007;24:877–905. https://doi.org/10.1002/rob.20224.
[3] Lindsay MB, Moncur MC, Bain JG, Jambor JL, Ptacek CJ, Blowes DW. Geochemical and mineralogical aspects of sulfide mine tailings. Appl Geochem 2015;57:157–77. https://doi.org/10.1016/j.apgeochem.2015.01.009.
[4] Olías M, Nieto JM, Sarmiento AM, Cerón JC, Canovas CR. Seasonal water quality variations in a river affected by acid mine drainage: the Odiel river (south west Spain). Sci Total Environ 2004;333:267–81. https://doi.org/10.1016/j.scitotenv.2004.05.012.
[5] Sanchez-España J, Llin A, Yusta I. Metallic copper (Cu[0]) obtained from Cu2+ rich acidic mine waters by two different reduction methods: crystallographic and geochemical aspects. Minerals 2022;12:322. https://doi.org/10.3390/min12030322.
[6] Sarmiento AM, Nieto JM, Olías M, Cánovas CR. Hydrochemical characteristics and seasonal influence on the pollution by acid mine drainage in the Odiel river basin (SW Spain). Appl Geochem 2009;24:697–714. https://doi.org/10.1016/j.apgeochem.2008.12.025.
[7] Sarmiento AM, Nieto JM, Casiot C, Elbaz-Poulichet F, Egal M. Inorganic arsenic speciation at river basin scale: the Tinto and odiel rivers in the iberian pyrite Belt, SW Spain. Environ Pollut 2009;157:1202–9. https://doi.org/10.1016/j.envpol.2008.12.002.
[8] Nieto JM, Sarmiento AM, Cánovas CR, Olías M, Ayora C. Acid mine drainage in the Iberian Pyrite Belt: 1. Hydrochemical characteristics and pollutant load of the Tinto and Odiel rivers. Environ Sci Pollut Res 2013;20:7509–19. https://doi.org/10.1007/s11356-013-1634-9.
[9] de la Torre ML, Grande JA, Valente T, Santisteban M, Cerón JC. Hydrochemical changes in a reservoir that receives water contaminated by acid mine drainage. Nord Hydrol 2015;46:303–12. https://doi.org/10.2166/nh.2014.114.
[10] de la Torre ML, Grande JA, Valente T, Pérez-Ostalé E, Santisteban M, Aroba J, Ramos I. Definition of redox and pH influence in the AMD mine system using a fuzzy qualitative tool (Iberian Pyrite Belt, SW Spain). Environ Sci Pollut Res 2016;23:5451–8. https://doi.org/10.1007/s11356-015-5718-6.
[11] Sarmiento AM, Grande JA, Luís AT, Dávila JM, Fortes JC, Santisteban M, Curiel J, de la Torre ML, Ferreira E. Negative pH values in an open-air radical environment affected by acid mine drainage. Characterization and proposal of a hydrogeochemical model. Sci Total Environ 2018;644:1244–53. https://doi.org/10.1016/j.scitotenv.2018.06.381.
[12] Amils R, González-Toril E, Aguilera A, Rodriguez N, Fernández-Remolar D, Diaz E, García-Moyano A, Sanz JL. Microbial ecology of a natural extreme acidic environment: lessons from Río Tinto. Adv Mater Res 2009;71–73:13–9. https://dx.doi.org/10.4028/www.scientific.net/AMR.71-73.13.
[13] Gonzalez-Toril E, Santofimia E, Lopez-Pamo E, Omoregie EO, Amils R, Aguilera A. Microbial ecology in extreme acidic pit lakes from the Iberian Pyrite Belt (SW Spain). Adv Mater Res 2013;825:23–7. https://dx.doi.org/10.4028/www.scientific.net/AMR.825.23.
[14] Nordstrom DK, Alpers CN. Geochemistry of acid mine waters. In: Plumlee GS, Logsdon MJ, editors. The environmental geochemistry of mineral Deposits, Rev. econ. geol., 6A; 1999. p. 133–60.
[15] Vaughan DJ, Coker VS. Biogeochemical redox processes of sulfide minerals. In: Ahmed IAM, Hudson Edwards KA, editors. Redox-reactive minerals: properties, reactions and applications in clean technologies, vol. 17; 2017. p. 95–119.
[16] Nordstrom DK, Southam G. Geomicrobiology of sulfide mineral oxidation. Rev Mineral 1997;35:361–90.
[17] San NO, Nazır H, Dönmez G. Microbially influenced corrosion and inhibition of nickel–zinc and nickel–copper coatings by Pseudomonas aeruginosa. Corrosion Sci 2014;79:177–83. https://doi.org/10.1016/j.corsci.2013.11.004.
[18] Liu H, Xu D, Dao AQ, Zhang G, Lv Y, Liu H. Study of corrosion behavior and mechanism of carbon steel in the presence of Chlorella vulgaris. Corrosion Sci 2015;101:84–93. https://doi.org/10.1016/j.corsci.2015.09.004.
[19] Ekolu SO, Diop S, Azene F. Potentiodynamic polarization study of the corrosion characteristics of acid mine drainage. In: Ekolu SO, Dundu M, Gao X, editors. Proceedings of the first international conference on construction materials and structures; 2014. p. 1436–41.
[20] Bhunia P, Kim G, Baik C, Lee H. A strategically designed porous iron-iron oxide matrix on praphene for heavy metal adsorption. Chem Commun 2012;48:9888–90. https://doi.org/10.1039/C2CC35120J.
[21] Padmalatha R, Lavanya M. Erosion corrosion of materials in industrial equipment: a review. Chemelectrochem 2023. https://doi.org/10.1002/celc.202300152.
[22] Askari M, Aliofkhazraei M, Ghaffari S, Hajizadeh A. Film former corrosion inhibitors for oil and gas pipelines—a technical review. J Nat Gas Sci Eng 2018;58:92–114. https://doi.org/10.1016/j.jngse.2018.07.025.
[23] Rao M, Keiser J, Levy AV, Wang B. Mechanical behavior of erosion-corrosion scales on steels as characterized by single-particle impacts. Wear 1991;150:135–52.
[24] Yu H, Zheng YG, Yao ZM. The cavitation erosion and erosion-corrosion behavior of carbon steel in simulating solutions of three rivers of China. Mater Corros 2006;57:705–14. https://doi.org/10.1002/maco.200503958.
[25] Lavanya M, Ramachandra V, Rao P. Erosion corrosion control of 6061 aluminum alloy in multi-phase jet impingement conditions with eco-friendly green inhibitor. Chin J Chem Eng 2020;28:340–7. https://doi.org/10.1016/j.cjche.2019.07.016.
[26] Bordeasu I, Ghiban B, Micu LM, Luca AN, Demian AM, Istrate D. The influence of heat aging treatments on the cavitation erosion behavior of type 6082 aluminum alloy. Materials 2023;26. https://doi.org/10.3390/ma16175875.